Supplemental Fig. S1

A

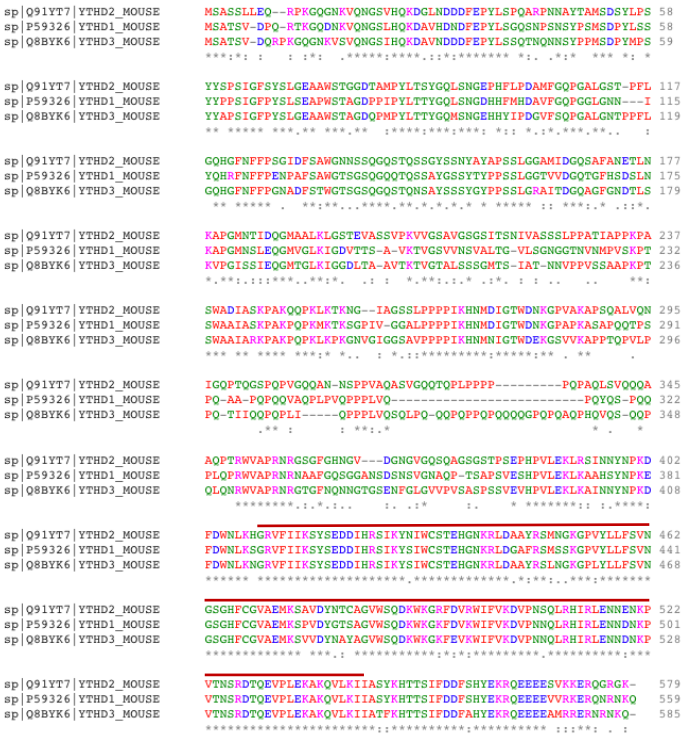

B

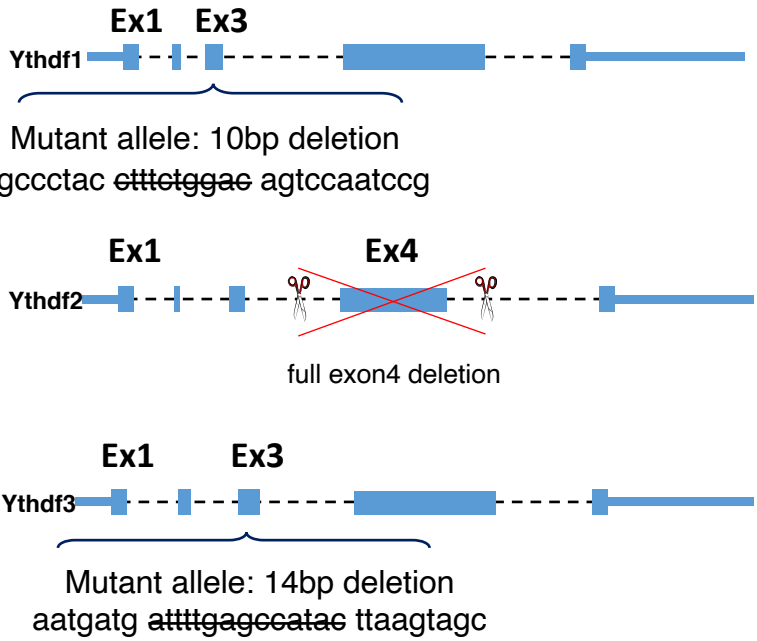

C

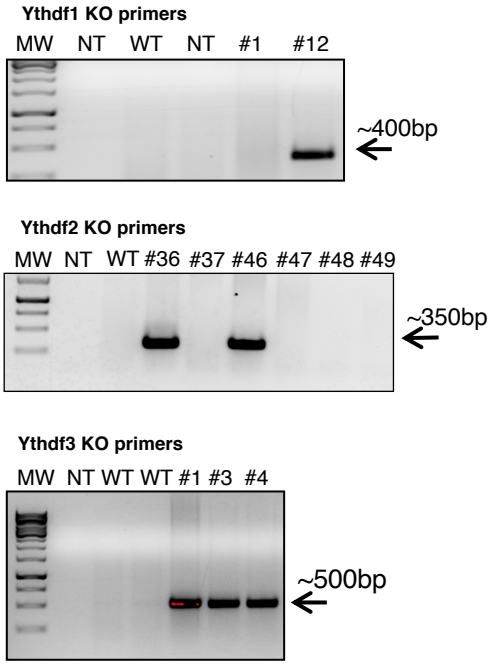

Supplemental Fig. S2

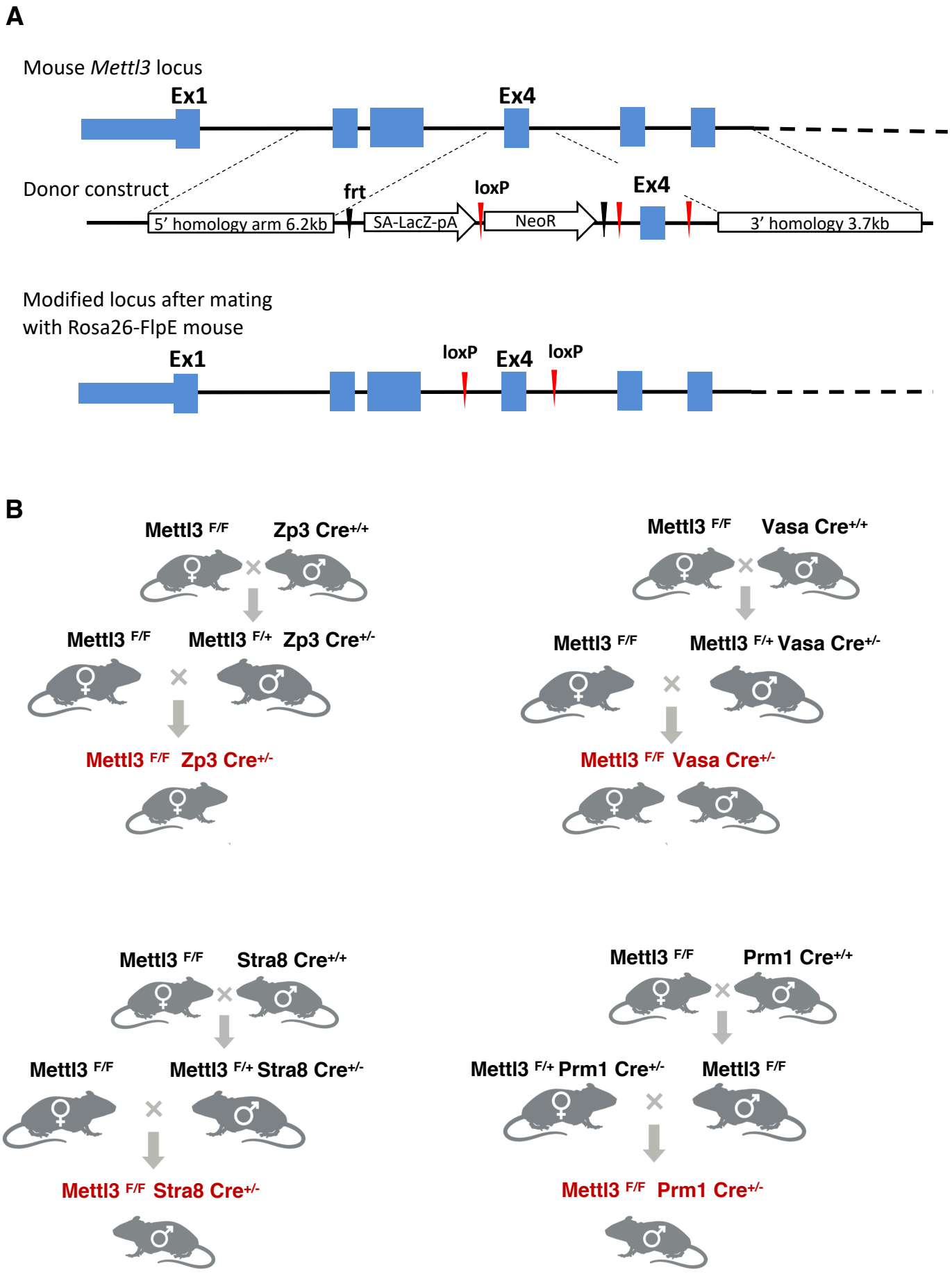

Supplemental Fig. S3

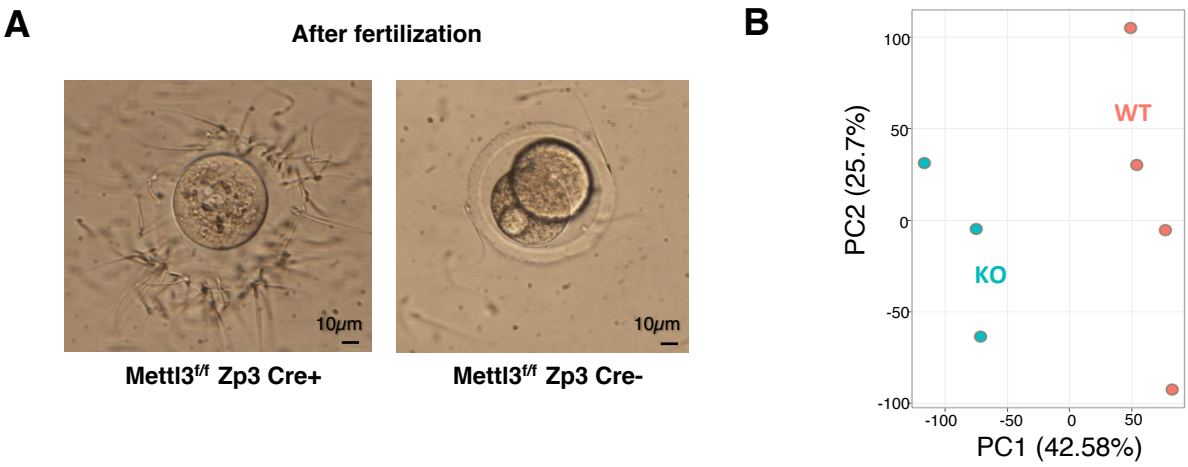

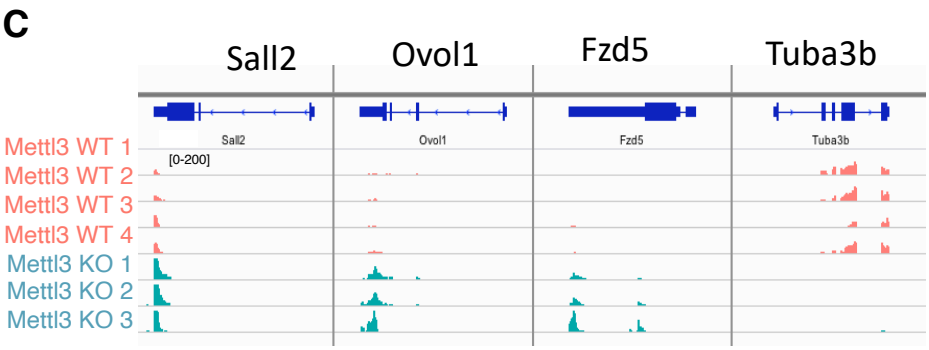

Supplemental Fig. S4

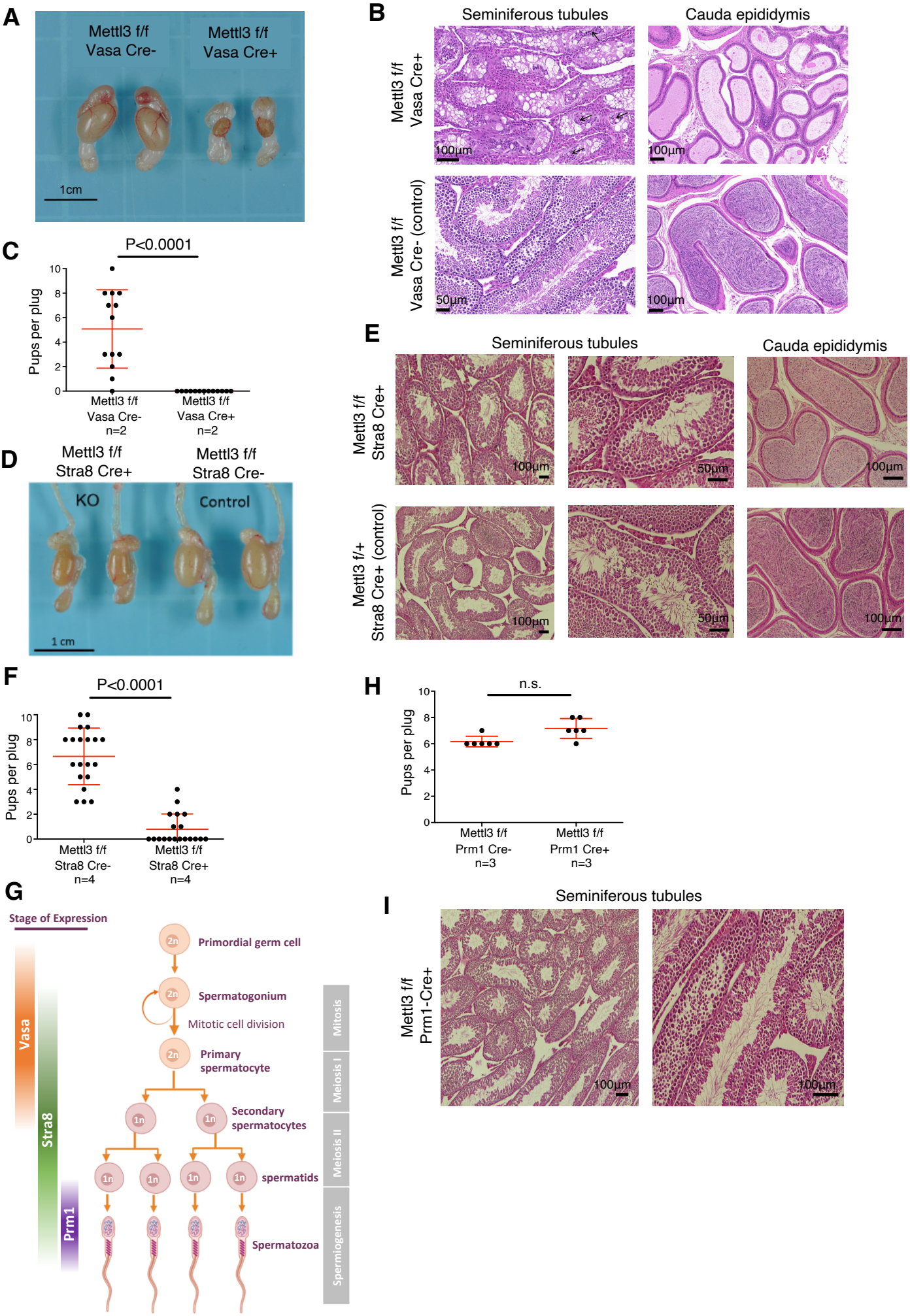

Supplemental Fig. S5

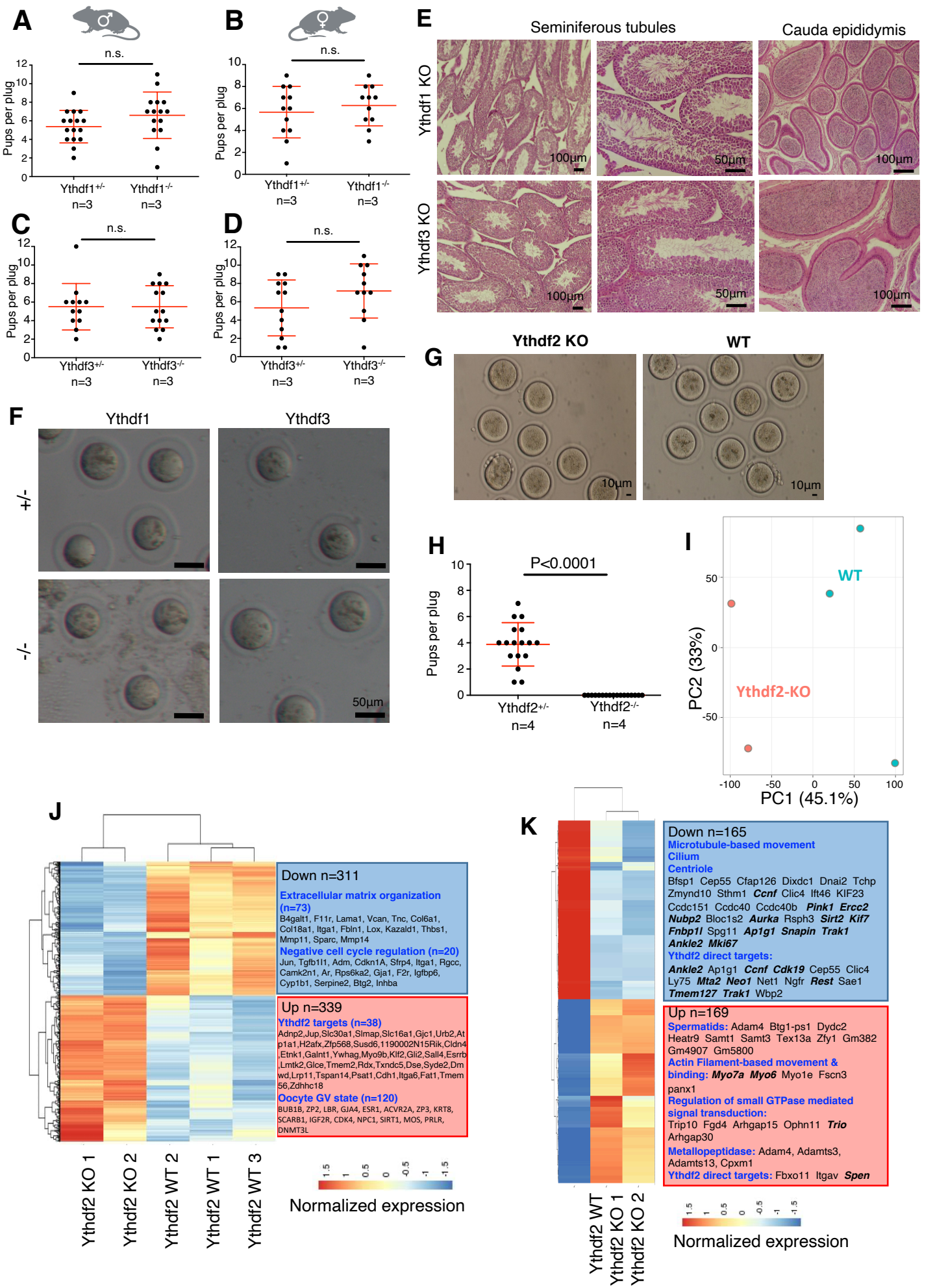

Supplemental Fig. S6

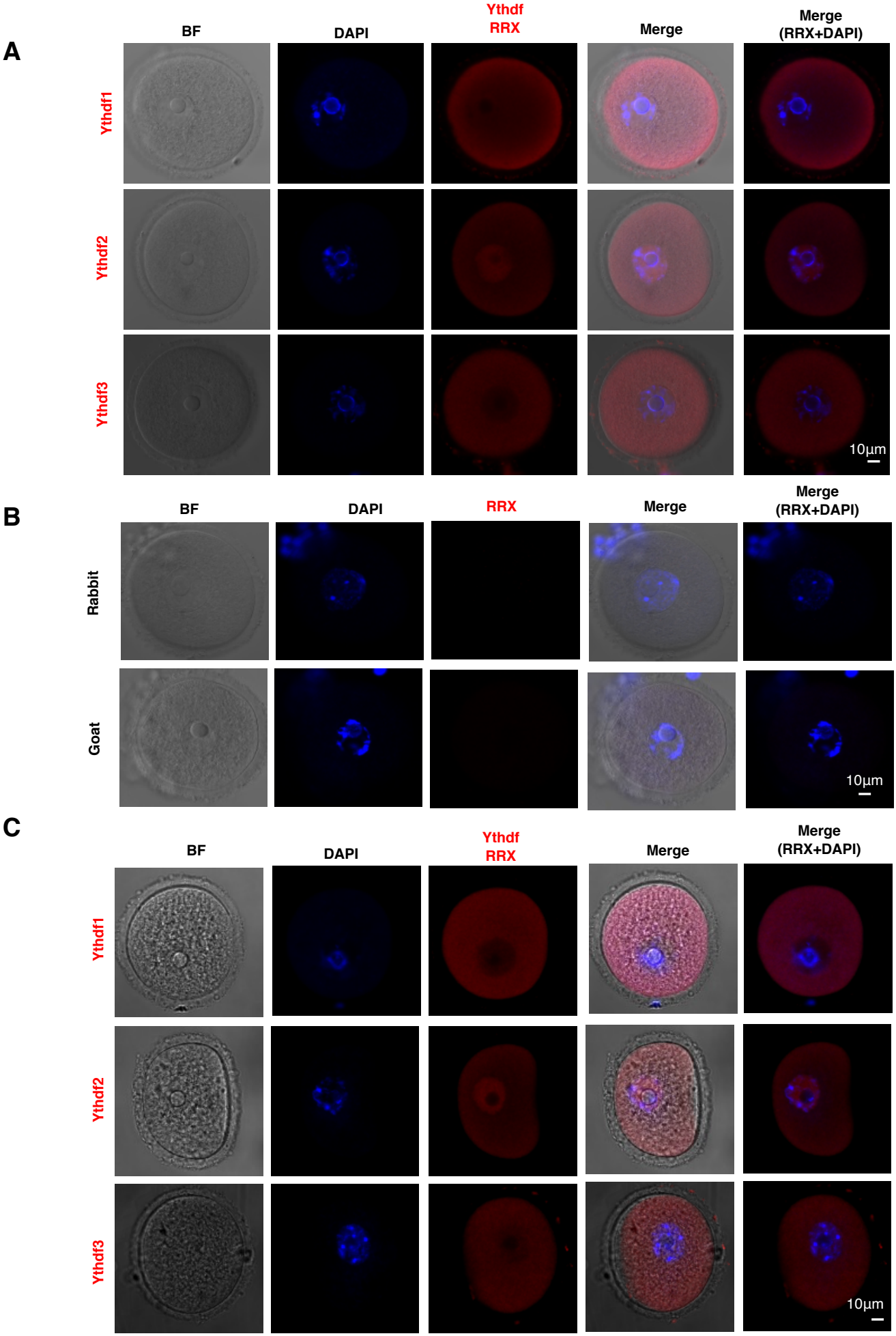

Supplemental Fig. S7

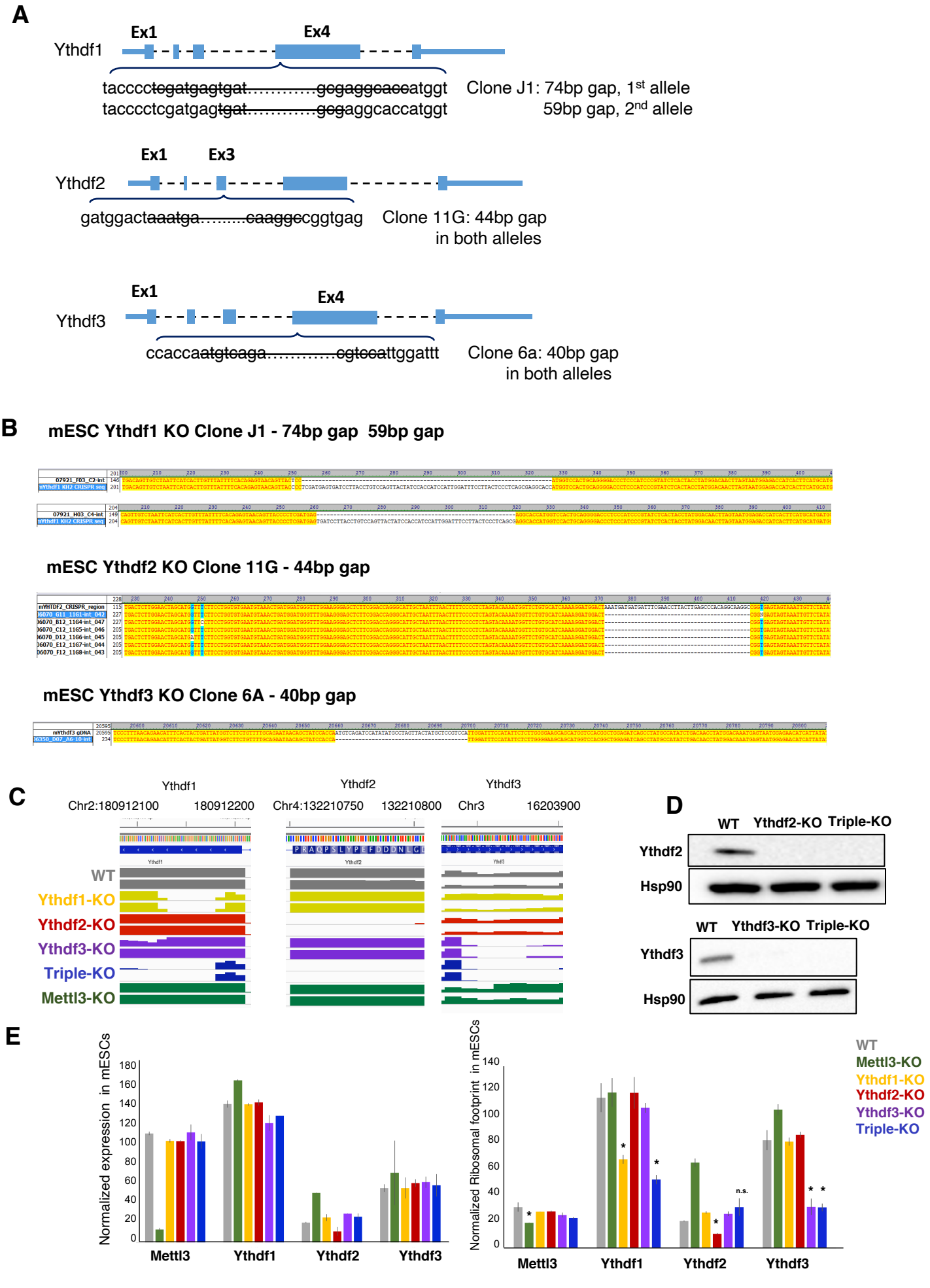

Supplemental Fig. S8

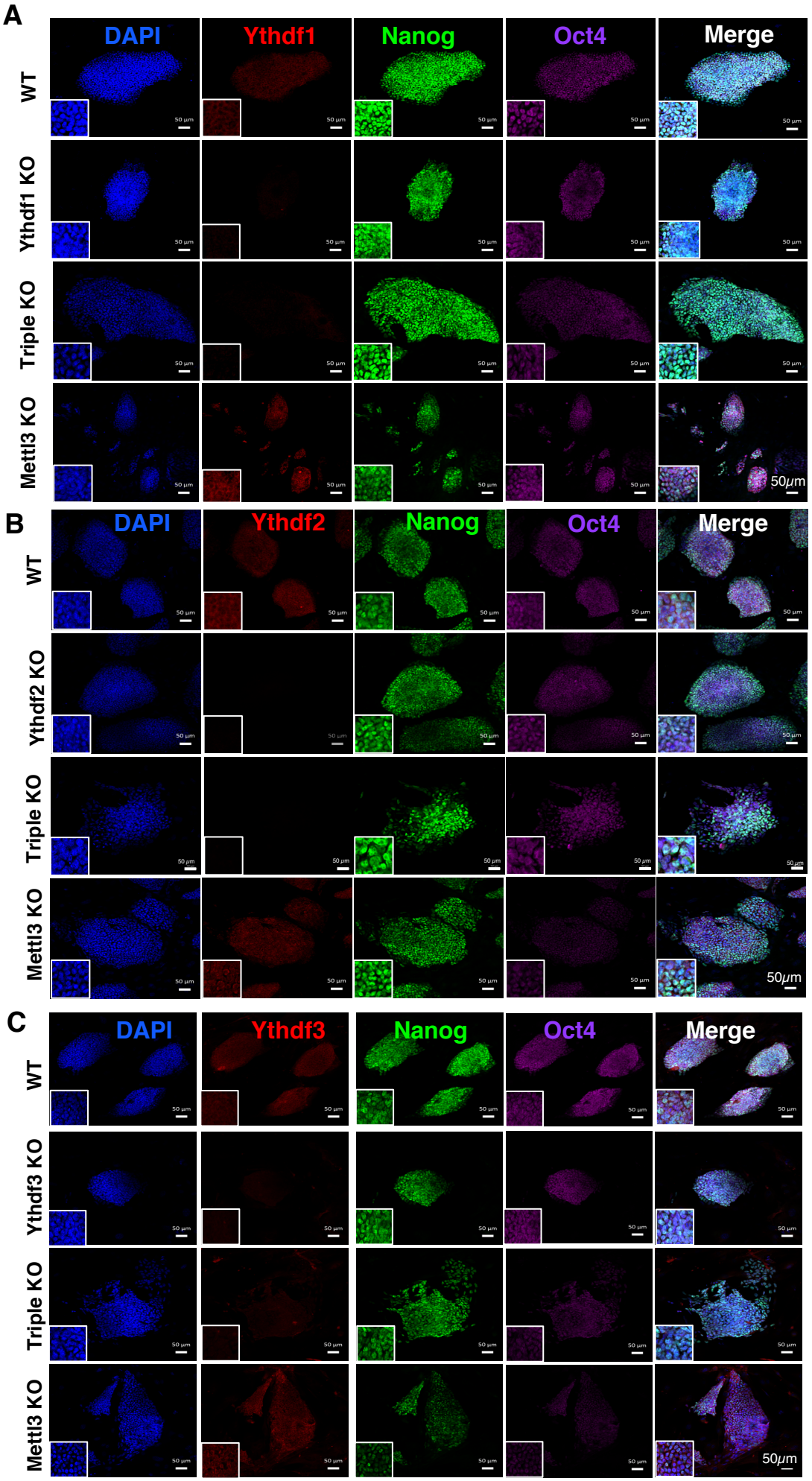

Supplemental Fig. S9

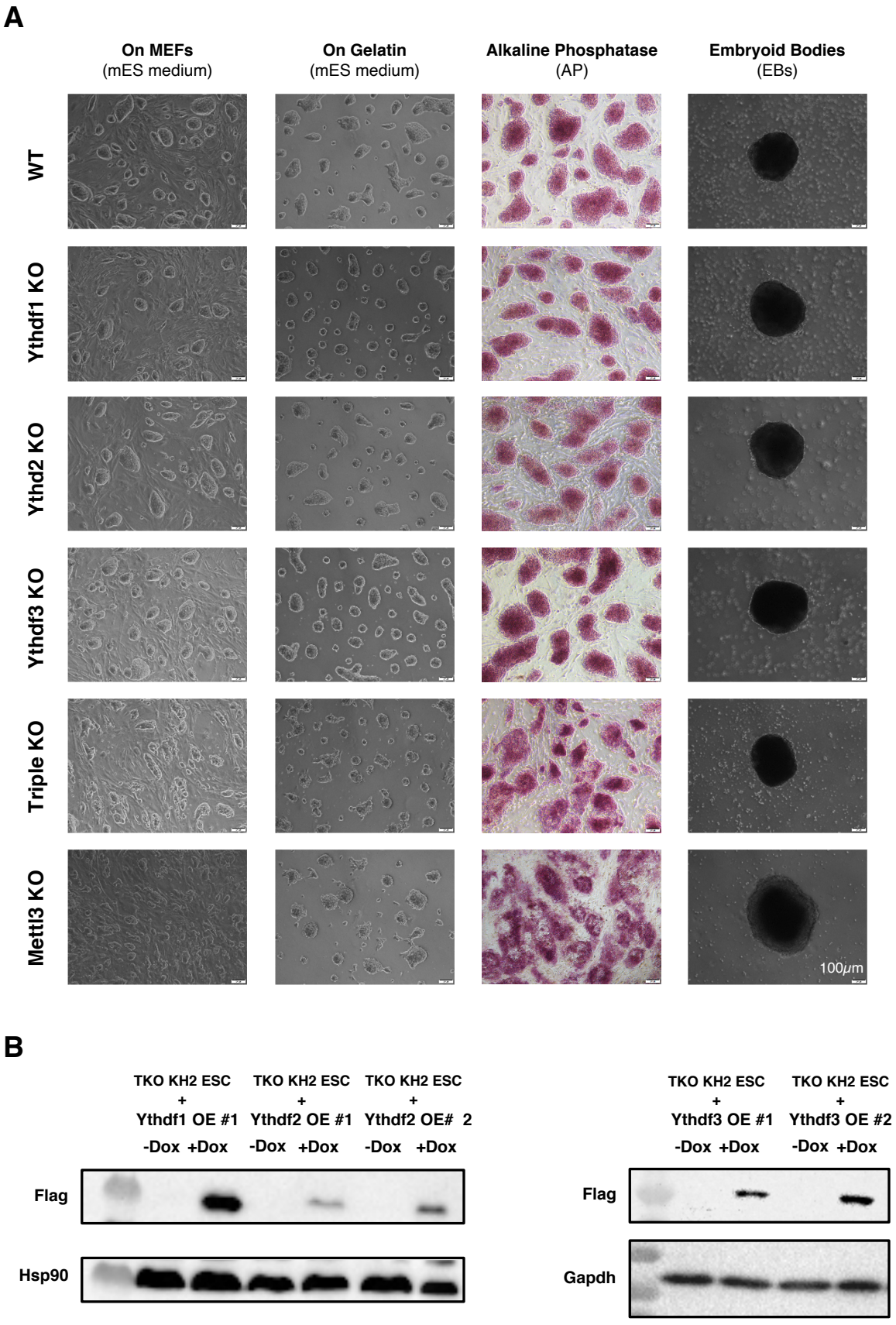

Supplemental Fig. S10

A

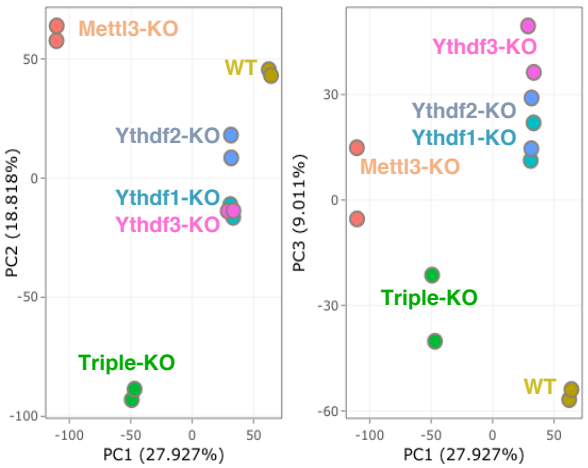

B

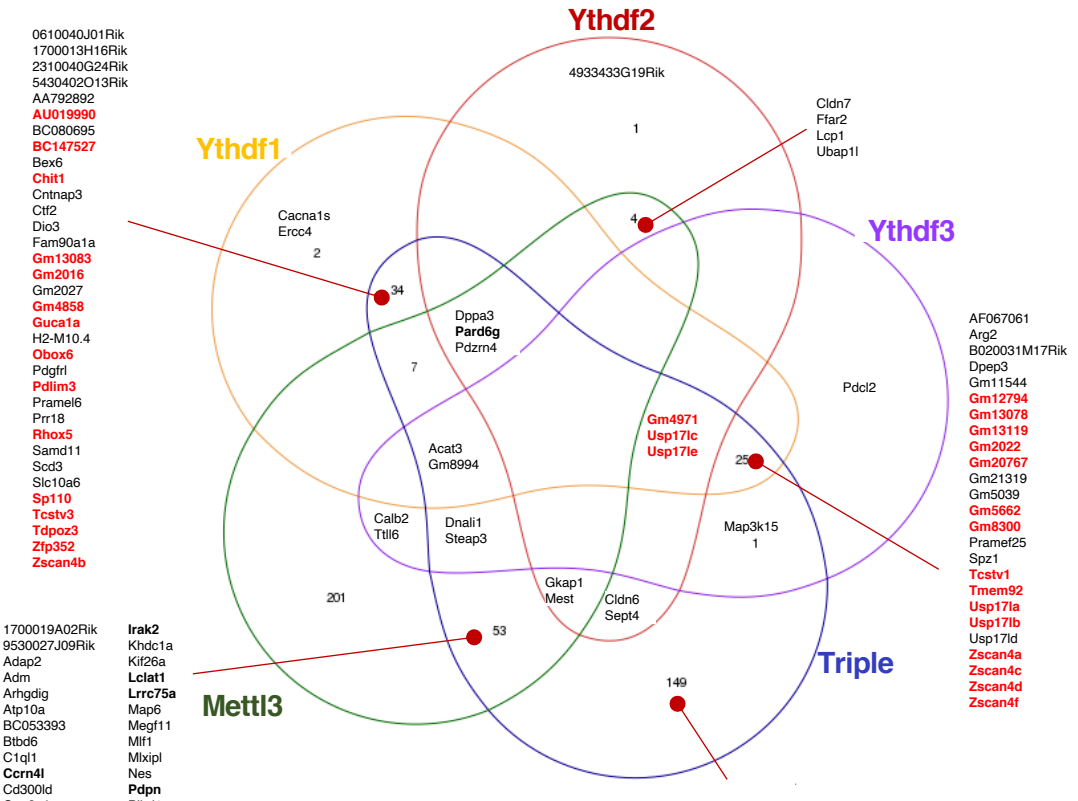

Supplemental Fig. S11

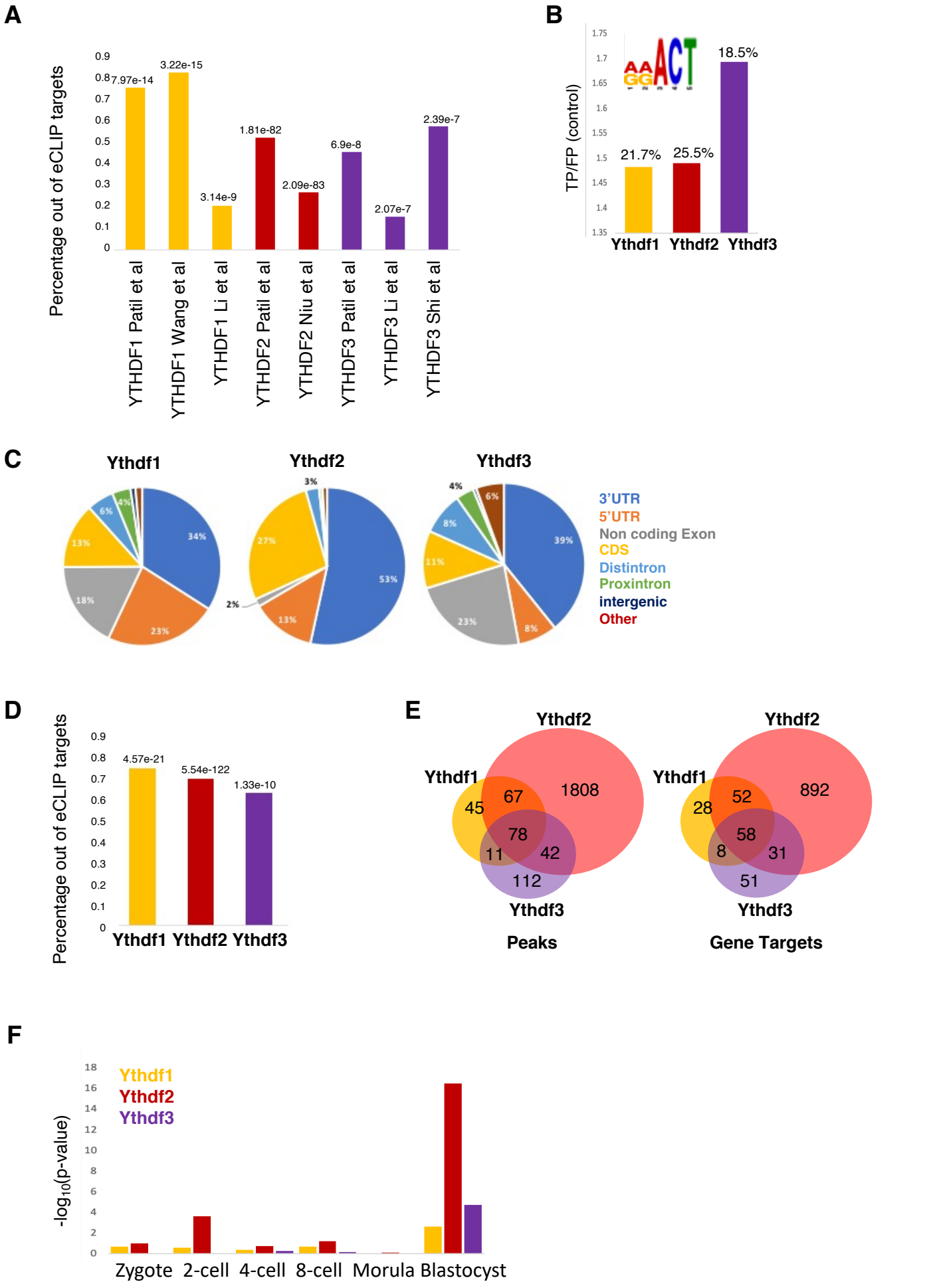

Supplemental Fig. S12

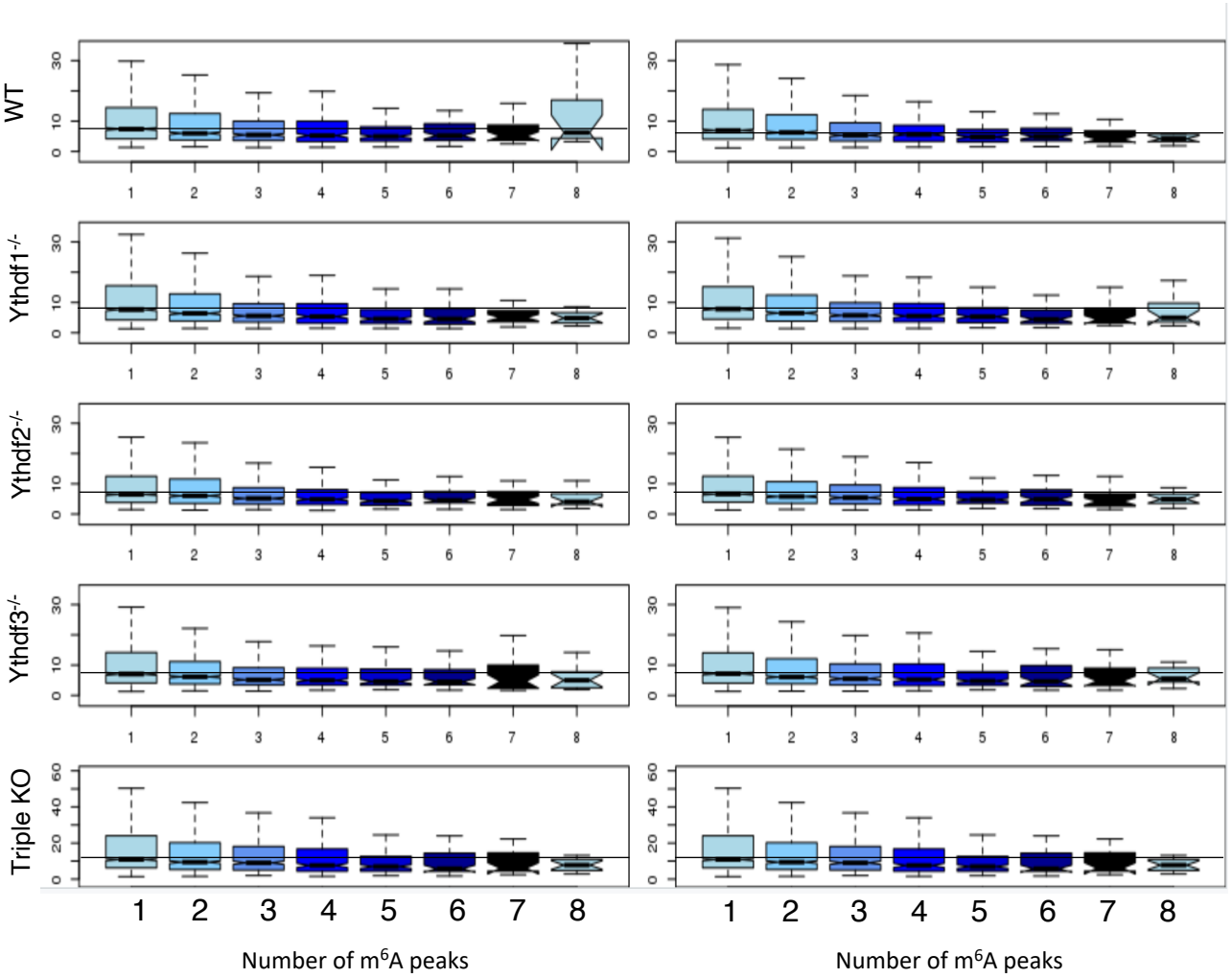

Supplemental Figure Legends

Supplemental Figure S1. Generating Ythdf1-KO, Ythdf2-KO and Ythdf3-KO mice.

A) Multiple alignments of Ythdf1, Ythdf2 & Ythdf3 proteins, calculated using the Clustal Omega tool. The area of YTH-domain is highlighted in red. Ythdf1-Ythdf3 protein sequence similarity is 70.11%, Ythdf1-Ythdf2 is 67.15%, and Ythdf2-Ythdf3 is 67.78%.
B) CRISPR-Cas9 targeting strategy for knocking-out Ythdf readers *in vivo* in mouse zygotes.
C) KO validation using PCR, showing successful primer integration in clones #12 (Ythdf1); #36, #46 (Ythdf2); #1, #3 & #4 (Ythdf3).

Supplemental Figure S2. Generating Mettl3 conditional knockout mouse model.

A) Targeting strategy for generating Mettl3$^{f/f}$ mice.
B) Crossing strategy for generating different Mettl3$^{f/f}$ Cre+ mice.

Supplemental Figure S3. Mettl3 is essential for female mice fertility.

A) *In vitro* fertilization of Mettl3$^{f/f}$ Zp3 Cre- control oocytes with WT sperm, leads to creation of two-cell stage embryos, while the Mettl3$^{f/f}$ Zp3 Cre+ oocytes fail to do so.
B) PCA of transcriptional profile of Mettl3$^{f/f}$ Zp3 Cre- and Mettl3$^{f/f}$ Zp3 Cre+ oocytes, showing a distinct expression pattern.
C) RNA-seq landscape of selected differential genes, generated with IGV browser. Normalized coverage is presented.

Supplemental Figure S4. Mettl3 and Ythdf2 are essential for male mice fertility.

A) Gross morphology of testis and epididymis of Mettl3$^{f/f}$ Vasa Cre+ and Mettl3$^{f/f}$ Vasa Cre- males. Cre+ males show a massive decrease in testis and epididymis size compared to Cre- control.
B) H&E staining showing severe degenerative changes in the seminiferous tubules of Mettl3$^{f/f}$Vasa Cre+ and lack of sperm in the cauda epididymis.
C) Number of pups per plug produced by Mettl3$^{f/f}$ Vasa Cre+ males, compared to Mettl3$^{f/f}$ Vasa Cre- control males. The mothers in both cases were WT. In this case there is a significant hypo fertility of the KO ($p<0.0001$, Mann-Whitney test).
D) Gross morphology of testis and epididymis of Mettl3$^{f/f}$ Stra8 Cre+ and Mettl3$^{f/f}$ Stra8 Cre- males. Cre+ males show a reduced-size testis and epididymis compared to Cre- control.
E) H&E staining showing mild degenerative changes in the seminiferous tubules of Mettl3$^{f/f}$Stra8 Cre+ and ~75% reduction in sperm quantity in the cauda epididymis, compared to Mettl3$^{f/+}$Stra8 Cre+ sibling control.
F) Same as in (C), for Stra8 Cre, showing a significant hypo fertility of the KO ($p<0.0001$, Mann-Whitney test).
G) Vasa, Stra8 and Prm1 are expressed during spermatogenesis, in different stages, as indicated.

H) Same as in (C), for Prm1 Cre, showing no significant difference between Cre+ and Cre- male fertility.
I) H&E staining of seminiferous tubules showing a normal morphology in Mettl3$^{f/f}$Prm1 Cre+ males.

Supplemental Figure S5. Ythdf1 knockout and Ythdf3 knockout mice are viable and fertile.

A) Number of pups per plug produced by mating Ythdf1-KO males, compared to Ythdf1-HET males. The mothers in both cases are WT. Here there is no significant difference between KO and HET male fertility (Mann-Whitney test).
B) Number of pups per plug produced by mating Ythdf1-KO females, compared to Ythdf1-HET females. The fathers in both cases are WT. Here there is no significant difference between KO and HET female fertility (Mann-Whitney test).
C) Number of pups per plug produced by mating Ythdf3-KO males, compared to Ythdf3-HET males. The mothers in both cases are WT. Here there is no significant difference between KO and HET male fertility (Mann-Whitney test).
D) Number of pups per plug produced by mating Ythdf3-KO females, compared to Ythdf3-HET females. The fathers in both cases are WT. Here there is no significant difference between KO and HET female fertility (Mann-Whitney test).
E) H&E staining of seminiferous tubules showing a normal morphology in Ythdf1-KO and Ythdf3-KO males.
F) The morphology of Ythdf1-KO and Ythdf3-KO flushed oocytes appears to be normal, similar to the Ythdf1-heterozygous (HET) and Ythdf3-HET flushed oocytes.
G) The morphology of Ythdf2-KO flushed oocytes appears to be normal, similar to the WT flushed oocytes.
H) Number of pups per plug produced by mating Ythdf2$^{-/-}$ females, compared to Ythdf2$^{+/-}$ control females. The fathers in both cases are WT. A significant difference between the fertility of KO and heterozygous females is observed ($p<0.0001$, Mann-Whitney test).
I) PCA of transcriptional profile of Ythdf2-KO and WT oocytes, showing a distinct expression pattern.
J) Transcriptional profile of genes that are differentially expressed between Ythdf2-KO and WT oocytes, along with selected enriched categories; 311 downregulated in KO, and 339 upregulated in KO.
K) Transcriptional profile of genes that are differentially expressed between Ythdf2-KO and WT round spermatids, along with selected enriched categories. m^{6}A-methylated genes appear in bold; 145 downregulated in KO, and 156 upregulated in KO.

Supplemental Figure S6. Oocytes staining for Ythdf1, Ythdf2 and Ythdf3 proteins.

A) Immunostaining of Ythdf1, Ythdf2 and Ythdf3 in ICR WT oocytes after hormone priming (PMS & hCG). More expanded presentation of images shown in Figure 1B.
B) Immunostaining of Ythdf1, Ythdf2 and Ythdf3 in ICR WT oocytes after PMS & HCG - negative control (NC), without primary antibody.
C) Immunostaining of Ythdf1, Ythdf2 and Ythdf3 in ICR WT oocytes without hormone priming.

Supplemental Figure S7. Generation and validation of Ythdf1/2/3 knockout mESC lines.

A) CRISPR-Cas9 targeting strategy for knocking out Ythdf readers in mESC cell lines.
B) Sequencing validation of the single-KO lines selected for further validation and analysis.
C) IGV browser view showing the missing fragments in the KO of Ythdf1, Ythdf2 & Ythdf3.
D) Western blot analysis for Ythdf2 and Ythdf3 in WT, single-KO and triple-KO mES cell lines.
E) Left: Normalized expression levels, Right: Normalized ribosomal footprint (ribo-seq) of Ythdf1,2&3 and Mettl3 proteins in the indicated mES cell lines. Translation of KO proteins is typically significantly lower compared to WT control (* t-test <0.05).

Supplemental Figure S8. Immunostaining of Ythdf1/2/3 KO mESC lines for pluripotency markers.

A) Immunostaining of Ythdf1 (red), Nanog (green), Oct4 (purple) and DAPI (blue) in WT, Ythdf1-KO, Triple-KO and Mettl3-KO cells.
B) Immunostaining of Ythdf2 (red), Nanog (green), Oct4 (purple) and DAPI (blue) in WT, Ythdf2-KO, Triple-KO and Mettl3-KO cells.
C) Immunostaining of Ythdf3 (red), Nanog (green), Oct4 (purple) and DAPI (blue) in WT, Ythdf3-KO, Triple-KO and Mettl3-KO cells.

Supplemental Figure S9. Morphology of Ythdf knockout mESC lines.

A) Phase and alkaline phosphatase (AP) staining of WT, single-KOs and Triple-KO mESCs, and phases of their EBs.
B) Triple-KO ESCs were rendered transgenic for either one of the Ythdf proteins under DOX induced promoter. Western blot of correctly targeted rescued lines showing the over expression (OE) of Ythdf1/2/3 proteins that can be induced by Dox, on the background of triple-KO cell line.

Supplemental Figure S10. Overlap of ESC signatures.

A) PCA clustering of KO and WT mESCs samples, showing that in PC1, single reader KO samples are closer to WT, compared to triple-KO and Mettl3-KO.
B) Overlap between upregulated gene signatures, measured in Ythdf single-KO and triple-KO, and in Mettl3-KO. Genes that are m^6A-methylated are bold. Genes that are two-cell markers are highlighted in red.

Supplemental Figure S11. CLIP data evaluation of Ythdf proteins.

A) Targets of Ythdf1, Ythdf2 and Ythdf3 highly overlap targets that were published before in human cancer cell lines.
B) Enrichment of RRACT (R=G/A) motif among binding peaks of Ythdf readers. Bars indicate enrichment ratio (True positive/False positive), numbers indicate the percentage of peaks which contain the motif.
C) Distribution of Ythdf peaks in various genomic entities, showing that the three readers have a tendency to bind 3' UTR, particularly Ythdf2.
D) Significant overlap of Ythdf targets, with m^6a-methylated genes.
E) Significant overlap between Ythdf1, Ythdf2 and Ythdf3 targets

F) Enrichment of Ythdf targets that were identified in mESCs, to early embryo genes (Gao et al. 2017), showing significant overlap with blastocyte genes.

Supplemental Figure S12. mRNA half-life as a function of number of m^6A peaks

The half-life of m^6A genes is plotted as a function of m6A peak number in the transcript, showing a slight yet significant decrease in half-life (shorter), as the number of m^6A peaks increase.

Supplemental Table Legends

Supplemental Table S1. Differentially expressed genes in gametogenesis KO experiments: Mettl3-KO oocytes, and Ythdf2-KO oocytes and spermatoids, compared to matched controls.

Supplemental Table S2. Differentially expressed genes in mESCs, that carry a single-KO (Ythdf1, Ythdf2, Ythdf3 or Mettl3) or triple-KO (Ythdf1/2/3), compared to WT controls.

Supplemental Table S3. eCLIP binding targets of Ythdf1, Ythdf2 and Ythdf3, measured in mESCs.

Supplemental Table S4. Normalized expressed along with transcript half-life, calculated for each gene in the single-KO (Ythdf1, Ythdf2, Ythdf3), triple-KO Ythdf1/2/3, and WT control.